



OPEN ACCESS

EDITED BY

Naveen Kumar Reddy Bogireddy,
National Autonomous University of Mexico,
Mexico

REVIEWED BY

Vanessa Maybeck,
Helmholtz Association of German Research
Centres (HZ), Germany
Cheng-Hung Chang,
National Yang Ming Chiao Tung University,
Taiwan

*CORRESPONDENCE

Hayder Amin,
✉ hayder.amin@dzne.de

RECEIVED 22 February 2024

ACCEPTED 27 August 2024

PUBLISHED 04 September 2024


CITATION

Hu X, Emery BA, Khanzada S and Amin H (2024)
DENOISING: Dynamic enhancement and noise
overcoming in multimodal neural observations
via high-density CMOS-based biosensors.
Front. Bioeng. Biotechnol. 12:1390108.
doi: 10.3389/fbioe.2024.1390108

COPYRIGHT

© 2024 Hu, Emery, Khanzada and Amin. This is
an open-access article distributed under the
terms of the [Creative Commons Attribution
License \(CC BY\)](https://creativecommons.org/licenses/by/4.0/). The use, distribution or
reproduction in other forums is permitted,
provided the original author(s) and the
copyright owner(s) are credited and that the
original publication in this journal is cited, in
accordance with accepted academic practice.
No use, distribution or reproduction is
permitted which does not comply with these
terms.

DENOISING: Dynamic enhancement and noise overcoming in multimodal neural observations via high-density CMOS-based biosensors

Xin Hu¹, Brett Addison Emery¹, Shahrukh Khanzada ¹ and Hayder Amin^{1,2*}

¹Group of Biohybrid Neuroelectronics (BIONICS), German Center for Neurodegenerative Diseases (DZNE), Dresden, Germany, ²TU Dresden, Faculty of Medicine Carl Gustav Carus, Dresden, Germany

Large-scale multimodal neural recordings on high-density biosensing microelectrode arrays (HD-MEAs) offer unprecedented insights into the dynamic interactions and connectivity across various brain networks. However, the fidelity of these recordings is frequently compromised by pervasive noise, which obscures meaningful neural information and complicates data analysis. To address this challenge, we introduce DENOISING, a versatile data-derived computational engine engineered to adjust thresholds adaptively based on large-scale extracellular signal characteristics and noise levels. This facilitates the separation of signal and noise components without reliance on specific data transformations. Uniquely capable of handling a diverse array of noise types (electrical, mechanical, and environmental) and multidimensional neural signals, including stationary and non-stationary oscillatory local field potential (LFP) and spiking activity, DENOISING presents an adaptable solution applicable across different recording modalities and brain networks. Applying DENOISING to large-scale neural recordings from mice hippocampal and olfactory bulb networks yielded enhanced signal-to-noise ratio (SNR) of LFP and spike firing patterns compared to those computed from raw data. Comparative analysis with existing state-of-the-art denoising methods, employing SNR and root mean square noise (RMS), underscores DENOISING's performance in improving data quality and reliability. Through experimental and computational approaches, we validate that DENOISING improves signal clarity and data interpretation by effectively mitigating independent noise in spatiotemporally structured multimodal datasets, thus unlocking new dimensions in understanding neural connectivity and functional dynamics.

KEYWORDS

high-density microelectrode arrays, large-scale neural recordings, spike sorting, waveform clustering, neural circuits/networks, neural dynamics

1 Introduction

The intricate exploration of computational neural dynamics investigated through the coordinated activity of interconnected neural populations, especially within the hippocampus and olfactory bulb, has been a cornerstone of contemporary neuroscience research (Vyas et al., 2020). These regions, central to spatial contextual learning, episodic memory, and olfactory processing, demonstrate remarkable neuroplasticity and are key to understanding the complex interplay of neural circuits in cognitive functions (Bird and Burgess, 2008; Mori et al., 1999). The hippocampus, a hub for information flow and synaptic plasticity, is crucial for the formation and retrieval of memories. Its ability to undergo structural and functional modifications in response to stimuli underscores the dynamic nature of neural networks (Lisman et al., 2017). Similarly, the olfactory bulb (OB) serves as the initial stage of olfactory processing, transforming odorant signals into neural representations through its intricate layers and diverse neuronal interactions. The regions' unique capacity for adult neurogenesis offers a window into the mechanisms underlying sensory perception and memory integration (Kempermann et al., 2018; Lepousez et al., 2013).

Extracellular neural recordings have long been a fundamental tool in neuroscience, offering insights into the electrical activity of neurons in their native environment (Buzsáki et al., 2012). The evolution of microelectrode arrays (MEAs) has expanded the scope of these observations, facilitating the simultaneous recording of multiple neural signals. Among the MEA technologies, high-density CMOS-based biosensing platforms (HD-MEAs) stand out due to their unparalleled technical capabilities (Berdondini et al., 2009; Müller et al., 2015). With the capacity to feature thousands of electrodes, these arrays can simultaneously capture a detailed panorama of neural activity across extensive networks, providing a dense sampling of electrical signals with high spatial and temporal resolution. This dense array structure allows for an in-depth analysis of neural interactions, offering a window into the synchronous and asynchronous patterns that underlie dynamical processes and functional connectome in multimodal neural networks and circuits (Hu et al., 2022; Emery et al., 2023a; Amin et al., 2016; Amin et al., 2017a; Amin et al., 2017b). This technology has facilitated a shift from the study of isolated neural pathways to an integrative view of brain's functional networks, bridging gaps in our knowledge of how neuronal ensembles coordinate to produce complex behaviors and cognitive functions (Buzsáki, 2004). HD-MEAs significantly enhance brain slice studies, merging *ex vivo* biosensing precision with brain tissue complexity. This approach allows for detailed exploration of electrical spiking activity and rhythmic dynamics of local field potentials (LFPs) under controlled conditions, thus enabling researchers to investigate environmental factors, apply pharmacological agents, or introduce genetic modifications to elucidate their effects on neural activity (Hu et al., 2022; Emery et al., 2023a; Amin et al., 2017b; Rossi et al., 2023; Emery et al., 2022; Emery et al., 2023b).

Despite advancements in these electrophysiological technologies, capturing the full spectrum of neural patterns within these complex networks remains challenging. The fidelity of extracellular neural recordings is frequently susceptible to a range of independent noise sources, including electrical interference from

the recording equipment, mechanical vibrations caused by external or internal laboratory factors, and environmental noise, such as electromagnetic fields. Removing noise from extracellular neural recordings poses several challenges due to the complex nature of neural signals and the non-stationary characteristics of noise. Neural signals often exhibit irregular firing patterns and non-Gaussian distributions, while noise can vary in amplitude and frequency content over time (Harris et al., 2000). Additionally, the presence of overlapping signals from multiple neuronal ensembles further complicates the task of noise removal. Several classical denoising strategies typically focused on temporal, spatial, or transform domains (i.e., Wavelet or Fourier) (Patil, 2015), which often fall short due to oversimplified assumptions about signal and noise characteristics (Donoho, 1995; Starck et al., 2002). The limited adaptability of these methods inadequately addresses the complexity and heterogeneity in large-scale neural recordings. This limitation not only impedes practical data analysis but also restricts our understanding of essential neural mechanisms.

Moreover, unsupervised denoising methods may introduce additional bias, as they might inadvertently emphasize or suppress certain signal features without ground truth verification, potentially leading to incorrect scientific inferences by distorting the underlying neural processes (Kay, 2022). Despite existing classical methods for denoising, current strategies do not effectively address the unique challenges posed by large-scale neural recordings captured by HD-MEAs. This gap underscores the critical need for new denoising approaches designed explicitly for HD-MEA data, which can dynamically adapt to its complexity, minimizing bias and significantly enhancing signal clarity for robust and accurate neural analysis.

In response to these challenges, we introduce DENOISING, a computational framework developed to transcend the limitations of conventional denoising techniques. Leveraging insights from recent studies highlighting the intricate dynamics and plasticity within the hippocampus and OB, DENOISING employs an adaptive engine to enhance the clarity and reliability of multidimensional neural recordings. Our method dynamically adjusts to the specific spatiotemporal characteristics (i.e., firing pattern statistics, network synchrony, burst, and waveform shapes) of extracellular signals and independent noise, facilitating a more nuanced separation of signal and noise components. Our approach is based on a deep understanding of the spatial and temporal structures of neural activity, informed by the complex interplay of vast neuronal ensembles within these critical brain regions. These dynamics are well-documented in the hippocampus (Lisman, 2005; Buzsáki, 1989; Scharfman, 2007; Bathellier et al., 2008; Luo and Katz, 2001) and the OB (Czanner et al., 2015; Gustafsson, 1996; Krishnan and Seelamantula, 2013) using various recording methodologies. This understanding supports the DENOISING method in identifying similar regions of activity as expected in both the hippocampus and the OB.

In the following sections, we detail our method's effectiveness through its use in analyzing large-scale neural LFP and spike data from complex hippocampal-cortical and olfactory networks. This includes demonstrating significant signal-to-noise ratio (SNR) (Czanner et al., 2015) enhancement, mapping topographical propagation features, classifying patterns based on their initiation and transmission, and waveform characteristics. Furthermore, we

benchmark DENOISING against traditional methods, demonstrating our approach's capacity to enhance data quality and reliability.

Our study illuminates the path toward more accurate and comprehensive analyses of HD-MEA's extracellular recordings, highlighting the potential to unlock new dimensions in our understanding of large-scale neural connectivity and functional dynamics and opening new avenues for exploring the mechanisms of learning, memory, and sensory processing.

2 Materials and methods

2.1 DENOISING framework

We employed an adaptive waveform-based thresholding technique designed specifically for processing signals captured by high-density CMOS-based microelectrode arrays. This involves setting customized thresholds for noise removal based on multiple signal waveform characteristics, including amplitude variations, frequency content, and waveform shape irregularities. The thresholding process is dynamically adjusted in real-time, leveraging the dense data acquisition capabilities of the arrays to detect and isolate noise components from true neural signals. The operational framework employed a composite of these signal features to define noise versus signal criteria, which are applied instantaneously to each waveform detected across the array's multiple recording channels. This method ensures a robust noise reduction while preserving the integrity of the biological signal, making it highly suitable for environments with variable noise conditions often encountered in high-density array recordings. To facilitate the application of our DENOISING method, the complete script, along with example datasets, is available on our GitHub repository (<https://github.com/HayderAminLab/DENOISING>). This resource includes detailed instructions for running the DENOISING method on both LFP-based and spike-based data acquired from HD-MEA systems, ensuring that other researchers can readily implement and validate our approach in their own studies.

2.2 Animals and acute brain slice preparation

Our study utilized 12-week-old female C57BL/6j mice (Charles River Laboratories, Germany), and ensured all procedures complied with European and national animal welfare regulations (Tierschutzgesetz), with approval license (Landesdirektion Sachsen; 25-5131/476/14). Brain slices were prepared according to our previous report (Hu et al., 2022; Emery et al., 2023a). Following anesthesia with 0.05% inhaled isoflurane (Primal, Germany), mice were decapitated, and their brains were extracted and submerged in a chilled sucrose solution for slicing. Using a Leica Vibratome VT1200S (Leica Microsystems, Germany), we prepared 300 μm thick horizontal brain slices, cut at 0°C–2°C in aCSF solution saturated with 95% O₂ and 5% CO₂ (pH = 7.2–7.4) of a high sucrose solution containing in mM: 250 Sucrose, 10 Glucose, 1.25 NaH₂PO₄, 24 NaHCO₃, 2.5 KCl, 0.5 Ascorbic acid, 4 MgCl₂, 1.2 MgSO₄, 0.5 CaCl₂. Furthermore, hippocampal and OB slices

were incubated for 45 min at 32°C and then allowed to recover for at least 1 h at room temperature before recording with HD-MEAs in a recording aCSF solution containing in mM: 127 NaCl, 2.5 KCl, 1.25 NaH₂PO₄, 24 NaHCO₃, 25 Glucose, 1.2 MgSO₄, 2.5 CaCl₂, and the solution was aerated with 95% O₂ and 5% CO₂.

2.3 Multimodal extracellular recordings and LFP/spike events detection

Extracellular neural activity was recorded using HD-MEAs crafted from complementary-metal-oxide-semiconductor (CMOS) technology, coupled with a bespoke acquisition system (3Brain AG, Switzerland). The CMOS chip featured 4,096 electrodes organized in a 64 × 64 array with a pitch of 42 μm , creating an active sensing area of approximately 7 mm², an ideal dimension for comprehensive recordings from both hippocampal-entorhinal cortex and olfactory bulb (OB) tissues at 14 kHz/electrode sampling frequency (Hu et al., 2022; Emery et al., 2023a). The on-chip amplification circuit allowed band-pass filtering from 1 Hz to 5 kHz, sufficient to record slow and fast neural activity. The hippocampal-entorhinal cortical recordings spanned six layers: dentate gyrus (DG), Hilus, CA3, CA1, entorhinal cortex (EC), and perirhinal cortex (PC). Similarly, OB recordings encompassed neuronal signals across five distinct layers: the olfactory nerve layer (ONL), glomerular layer (GL), external plexiform layer (EPL, we referred to as the projection layer), the olfactory cortex (OCx), and granule cell layer (GCL). Integration of a modular stereomicroscope (Leica Microsystems, Germany) allowed for simultaneous acute slice imaging and extracellular recording, facilitating the correlation of spatial tissue organization with electrode activity. Event detection for LFPs and multi-unit spiking activity (MUA) was conducted using commercial software (3Brain AG), where data was first refined by applying a low-pass filter (1–100 Hz) for LFPs and a band-pass filter (300–3,500 Hz) for MUA. Following the filtering, events were detected using hard thresholding alongside precise timing spike detection (PTSD) algorithms, respectively (Hu et al., 2022; Emery et al., 2023a). This sequence ensured that the frequency components suitable for describing LFPs and spikes were accurately isolated before event detection, improving the specificity and accuracy of the detected events.

2.4 Topographical spatiotemporal voltage maps, CATs, and event incidence

To assess the impact of DENOISING in enhancing dynamical spatiotemporal information in the hippocampus and OB subregional networks, we computed averaged LFP and spike event frequencies across their interconnected layers. By employing high-resolution, multimodal recordings, we generated dynamic topographical maps for LFP and spike data within respective 50 ms and 10 ms time bins. Illustrated in pseudo-color, these maps demonstrate the spatial distribution of electrical activity per event, accentuating the enhanced clarity of neuronal interactions after noise removal. Spatiotemporal activity propagation was quantified by analyzing the center of activity

trajectories (CATs) (Hu et al., 2022). Furthermore, we determined long-range event incidence rates and their distributions, leveraging simultaneous recordings from extensive subnetworks to clarify decontaminated initiation sites and their propagation across layers after employing DENOISING.

2.5 Traditional noise-removal methods

DENOISING was evaluated against established noise reduction techniques in neural recordings, categorized into signal and transform domain methods. In the signal domain, we applied one-dimension causal forward-in-time FIR filtering (Gustafsson, 1996) (<https://docs.scipy.org/doc/scipy/reference/generated/scipy.signal.lfilter.html#scipy.signal.lfilter>) and the Savitzky-Golay algorithm (Krishnan and Seelamantula, 2013) for smoothing the signal by fitting a polynomial to a segment of neural data points via least squares regression (https://docs.scipy.org/doc/scipy/reference/generated/scipy.signal.savgol_filter.html). For transform domain denoising, we utilized Wavelet (WT) and Fourier Transform (FT) methods, which transform the recorded signals into different frequency components, where the noise removal or filtering operation is applied more effectively. WT denoising involves convolution with a wavelet function to isolate signal frequencies computed using the PyWavelets package (<https://github.com/PyWavelets/pywt>). FT approaches modify signal frequencies in the frequency domain before an inverse transformation (<https://numpy.org/doc/stable/reference/generated/numpy.fft.ifft.html>). These methodologies provide a foundation to demonstrate DENOISING's performance extracting clean neural signals.

2.6 Extracellular waveform characterization and clustering assessment

We performed unsupervised clustering analysis to group similar waveform shapes of LFP patterns using principal component analysis (PCA) clustering with the mean-shift algorithm (Minka, 2008; Comaniciu and Meer, 2002). PCA was applied to reduce the dimensionality of the waveform data while preserving the essential features (<https://scikit-learn.org/stable/modules/generated/sklearn.decomposition.PCA.html>). The mean-shift algorithm was then employed to identify clusters in the reduced-dimensional space (<https://scikit-learn.org/stable/modules/generated/sklearn.cluster.MeanShift.html>). Unlike other algorithms, such as k-means (Coates and Ng, 2012), mean-shift does not require the number of clusters to be specified, as it automatically determines the clusters based on data density. This approach allowed us to uncover distinct patterns of LFP activity within the hippocampal and OB slices in raw and denoised data.

To identify and cluster spiking activity from the recordings, we employed an unsupervised spike sorting algorithm compatible with large-scale neural recordings (Hilgen et al., 2017) and available on GitHub (<https://github.com/mhhennig/HS2>). The spike sorting algorithm was modified and implemented to extract various features, such as spike waveforms, spike amplitudes, and spike timing, to isolate individual spikes and group them into distinct

clusters corresponding to different neuronal units estimated from multimodal large-scale neuronal ensembles. This process enabled us to differentiate between different types of firing electrodes and discern their spiking patterns within the hippocampal and OB slices.

Furthermore, we computed silhouette coefficients (SC) to assess the quality of the clustering results obtained from both LFP waveform shapes and multi-unit spiking activity (Rousseeuw, 1987). Silhouette coefficients measure the coherence and separation of clusters, providing a quantitative measure of clustering quality (https://scikit-learn.org/stable/auto_examples/cluster/plot_kmeans_silhouette_analysis.html). Higher silhouette coefficients indicate better-defined and more distinct clusters, while negative coefficients suggest overlapping or poorly separated clusters. By computing silhouette coefficients, we could objectively evaluate the effectiveness of our DENOISING method through clustering algorithms in capturing the underlying structure of the neural activity data compared to raw noise-contaminated data. This highlights the only actual partition of waveforms from the firing electrodes without the bias of the clustering algorithm used to obtain them.

2.7 Performance benchmark analysis

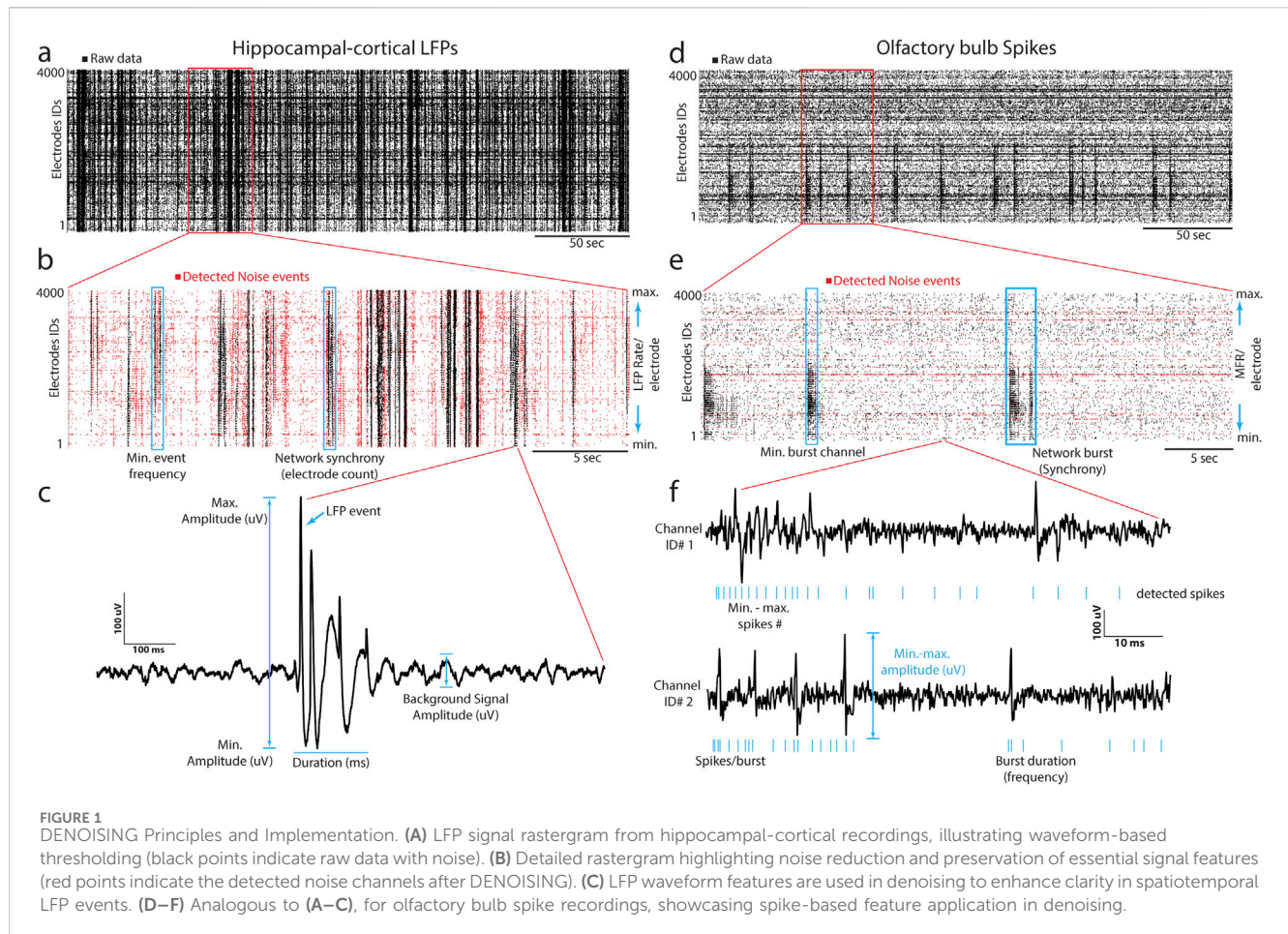
To evaluate the performance of DENOISING, we employed three metrics—a normalized signal-to-noise ratio difference (SNR_{DR}) (Czanner et al., 2015), SNR distribution (Lecoq et al., 2021) and root mean square noise (RMS) (Hyndman and Koehler, 2006). SNR_{DR} offers a normalized measure of improvement, facilitating meaningful comparisons even when baseline SNR levels vary widely between recordings. This metric highlights the relative gains achieved by our denoising method, providing insights into its efficiency in enhancing signal quality relative to the initial noise level. SNR distribution evaluates the performance of the denoising method across the entire large-scale network with high channel counts. It demonstrates the method's general applicability and effectiveness under diverse experimental conditions. RMS is a statistical measure that quantifies the magnitude of signal variation, assessing the effectiveness of noise reduction. This metric further quantifies improvements in signal quality, complementing the SNR metrics by offering a direct measure of the denoising impact on signal magnitude. The dynamic range of the SNR using the logarithmic decibel scale (SNR_S) is defined as:

$$\text{SNR}_{\text{Signal}}^{\text{dB}} = 10 \log_{10}(\text{SNR}_{\text{Signal}})$$

The normalized SNR_{DR} is defined as the normalized difference between the (SNR) of the denoised signal and the SNR of the raw signal, given as:

$$\text{SNR}_{\text{DR}} = \frac{(\text{SNR}_{\text{denoised}}^{\text{dB}} - \text{SNR}_{\text{raw}}^{\text{dB}})}{\text{SNR}_{\text{raw}}^{\text{dB}}} \times 100$$

In addition, to determine the distribution of SNR in large-scale recordings, we computed SNR as the ratio of mean firing activity in all active channels to standard deviation across the time domain.



Furthermore, the RMS measures the magnitude of the varying components of biosignals. It provides a single number that represents the noise level in a way comparable across raw and denoised conditions. The RMS is defined as:

$$\text{RMS noise} = \sqrt{\frac{\sum_{i=1}^N (x_i)^2}{N}}$$

Where x_i denotes the individual values of the firing electrodes (signals), and N represents the number of data samples.

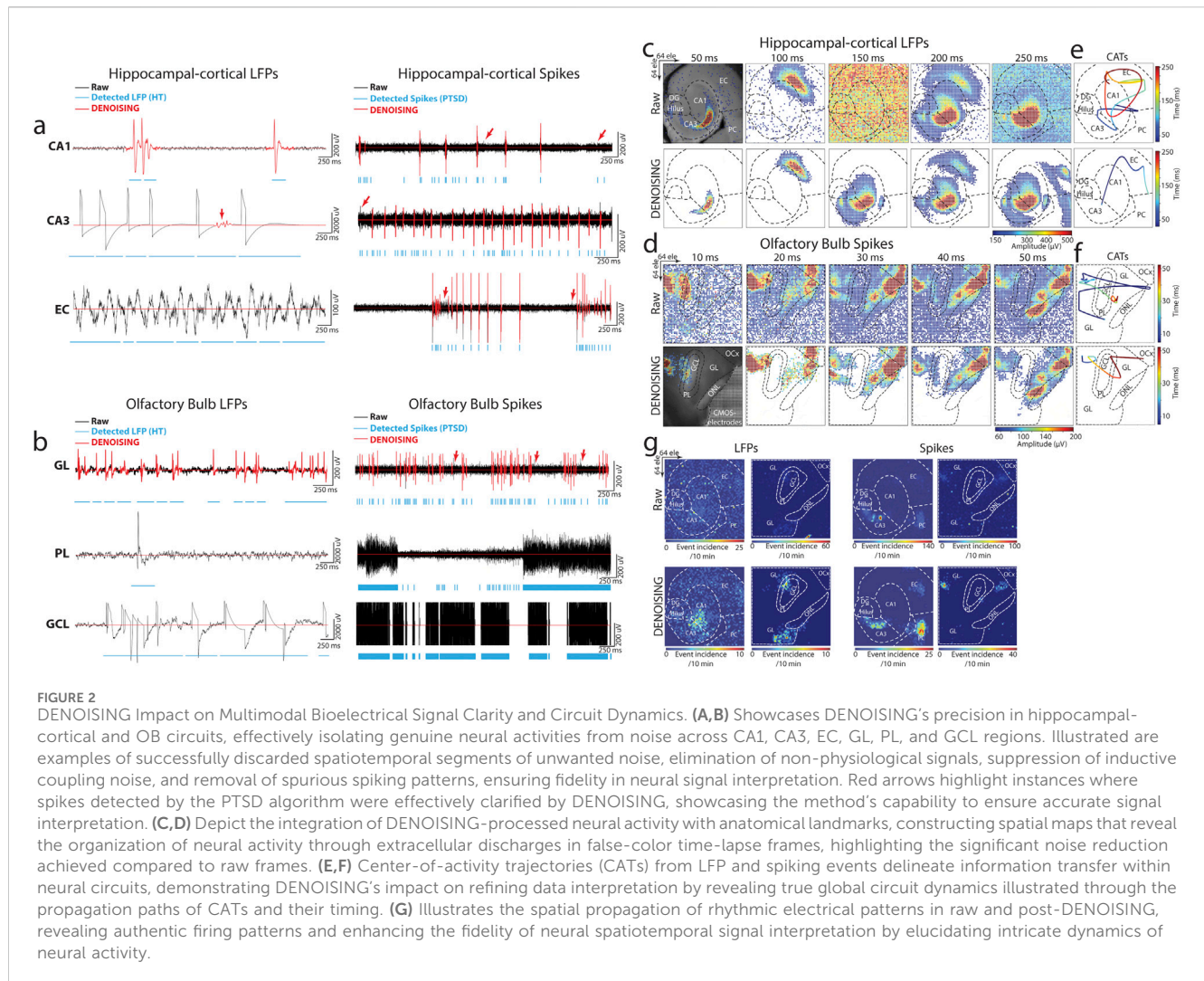
2.8 Data and statistical analysis

All analyses used in this study were developed and implemented with custom-written Python scripts available on our Lab's GitHub (<https://github.com/HayderAminLab/DENOISING>). Any employed packages are cited accordingly. All statistical analyses were performed with Python and Originlab 2022. All data in this work were expressed as the mean \pm standard error of the mean (SEM). Differences between groups were examined for statistical significance, where appropriate, using one-way analysis of variance (ANOVA) or Kolmogorov-Smirnov test followed by Tukey's posthoc testing. $p < 0.05$ was considered significant.

3 Results

3.1 DENOISING principles

We implemented the DENOISING method as a novel approach for denoising extracellular large-scale recordings obtained from hippocampal and olfactory bulb slices. The primary objective of our method was to effectively remove noise while preserving the essential features of the signals, thereby enhancing the clarity and precision of LFP and spike patterns (Figure 1). The method is implemented through waveform-based thresholding, which operates directly on the time-domain representation of the signals. This method involves setting a threshold level based on the characteristics of the waveforms and removing signal segments below this threshold, which are considered noise. We separately applied waveform-based thresholding to both LFP (Figures 1A–C) and spike (Figures 1D–F) signals to ensure optimal denoising performance for each signal type. The DENOISING method utilized several identifiers derived from network-wide features to enhance the noise-removal process and improve its adaptability to different datasets. These identifiers were used to set up a template containing specific values of spatiotemporal pattern features, which could be cast off for testing with other datasets. The network features included - firing frequency (synchrony), number of firing electrodes (adapted to the structural clusters identified by optical imaging



information combined with electrophysiology recordings), event duration (min-max range), event amplitude, and bursting frequency. Following the integration of denoising parameters and their automated application to the hippocampal and OB recorded datasets, the DENOISING method exhibited a substantial reduction in independent noise artifacts, as depicted in network-wide activity represented in 5-min raster plots (Figure 1).

3.2 Validation with multimodal neural recordings

To underscore the physiological validity of our neural recordings, we initially focused on exploiting multimodal neural recordings derived from extracellular LFP and spike signals within well-characterized hippocampal-cortical and olfactory bulb circuits (Hu et al., 2022; Emery et al., 2023a). These systems are known for their intricate spatiotemporal dynamics, including specific initiation sites and subsequent propagation across distinct neural layers. Such detailed mapping is crucial for understanding the complex interplay of neural activities that underpin cognitive and sensory processing

(Vyas et al., 2020; Bird and Burgess, 2008; Mori et al., 1999). We applied the DENOISING framework to process these recordings, intended not only to assess its noise reduction capabilities but also to demonstrate that our approach preserves the biological fidelity of these dynamic neural interactions.

Representative event traces from key regions of the hippocampal-cortical network regions (i.e., CA1, CA3, and EC) and OB (i.e., GL, PL, and GCL) were analyzed. These traces captured a diverse array of LFP and spike biosignal signatures both in their raw, unprocessed state and following noise reduction using DENOISING across multiple categories of noise examples (Figure 2). The significant denoising performance of our method for both LFP and multi-unit spiking-based patterns was demonstrated in—i) effectively discarded spatiotemporal segments of unwanted noise, even when the stringent hard threshold and PTSD algorithms detected events. This precision was evident in representative traces from CA1 and GL electrodes (Figures 2A, B), highlighting the method's ability to discern genuine neural activity from noise. ii) identified and eliminated non-physiological signals contaminated with independent noise, including 50 Hz environmental noise (Figure 2A; EC electrode

and mechanical artifacts stemming from perfusion glitches (Figure 2B; PL electrode). This capability underscores the method's robustness in preserving the fidelity of neural recordings. iii) suppressed inductive coupling noise originating from CMOS-chip electrical wiring before signal amplification. DENOISING enhanced the accuracy of neural signal interpretation by distinguishing and attenuating false signals with similar frequency and amplitude to neural oscillations, as evidenced by traces in (Figures 2A, B; CA3 and GCL electrodes). iv) removed falsely detected spurious spiking patterns embedded within the physiological spiking activity observed across electrodes in CA1, CA3, EC, and GL regions (Figures 2A, B). This ensures the extracted spiking activity reflects the true neuronal firing dynamics, facilitating more precise insights into neural circuit function and information processing within these critical brain regions. v) rectified false signal patterns that emerged from dysregulated chip calibration, as illustrated in traces from PL and GCL electrodes (Figure 2B). The auto-zeroing circuit integrated into the CMOS-chip, is regularly calibrated to the electrode's DC voltage, which could be impaired due to various noise sources and light effects, leading to signal contamination.

Next, to elucidate the profound impact of DENOISING in identifying and mitigating independent noise across the entire spatiotemporal functional landscape within our recorded subnetworks, we integrated large-scale activity with the brain network's anatomical landmarks. We overlaid the computed mean of firing patterns obtained from LFP and spike recordings onto optical images of hippocampal-cortical and OB circuits; then, we constructed maps that revealed the spatial organization of neural activity (Figures 2C, D). These maps encoded extracellular discharges in false-color time-lapse frames depicting full LFP and spiking events. The frames, with time steps of 50 ms for LFP and 10 ms for spiking events, showcased the global noise-embedded contamination across layers in raw data frames compared to the denoised frames. This visualization underscored the substantial reduction in noise achieved by DENOISING, enhancing the clarity and precision of the recorded neural activity. We further constructed center-of-activity trajectories (CATs) from LFP and spiking events to delineate information transfer and processing pathways within the neural circuits. A striking disparity between raw and denoised frames (in events time and amplitude) was observed in the averaged-CAT patterns, emphasizing the pivotal role of DENOISING in refining data interpretation and uncovering the true global circuit dynamics emerging from population activity (Figures 2E, F).

Simultaneous recordings from all multimodal network layers were leveraged to compute the generation site and trace the spatial propagation of rhythmic electrical patterns. This analysis illustrated the remarkable significance of DENOISING in providing clarity to unveil the authentic firing patterns obscured by noise in the raw data. The spatial maps of rhythmic electrical patterns elucidated the intricate dynamics of neural activity and highlighted the transformative effect of DENOISING in enhancing the fidelity of neural signal interpretation (Figure 2G).

In summary, the integration of robust DENOISING techniques with detailed spatial analyses significantly advances the interpretation of neural activity within key brain networks. This approach aligns functional insights with underlying neural

structures, enhancing signal clarity and ensuring that observed behaviors match known anatomical features. This synergy offers crucial insights into complex neural interactions and their physiological implications. These enhanced denoising capabilities could impact the understanding of prolonged depolarization states and the synchronization within neural networks, potentially offering new avenues for research into neural connectivity and its role in cognitive and sensory processing.

3.3 DENOISING for waveform characterization

Analysis of oscillatory activity waveforms is pivotal for understanding the diverse functionalities within neural circuits. Waveform shapes can indicate different types of neuronal activity and are vital in identifying distinct neuronal types in specific brain regions and their roles in processing information (Cole and Voytek, 2017). Accurately characterizing waveform features from large-scale neural recordings is essential for decoding the intricate activities within brain networks. This necessitates enhancing signal clarity through meticulous noise reduction, ensuring that the subtle nuances of neural interactions are not lost.

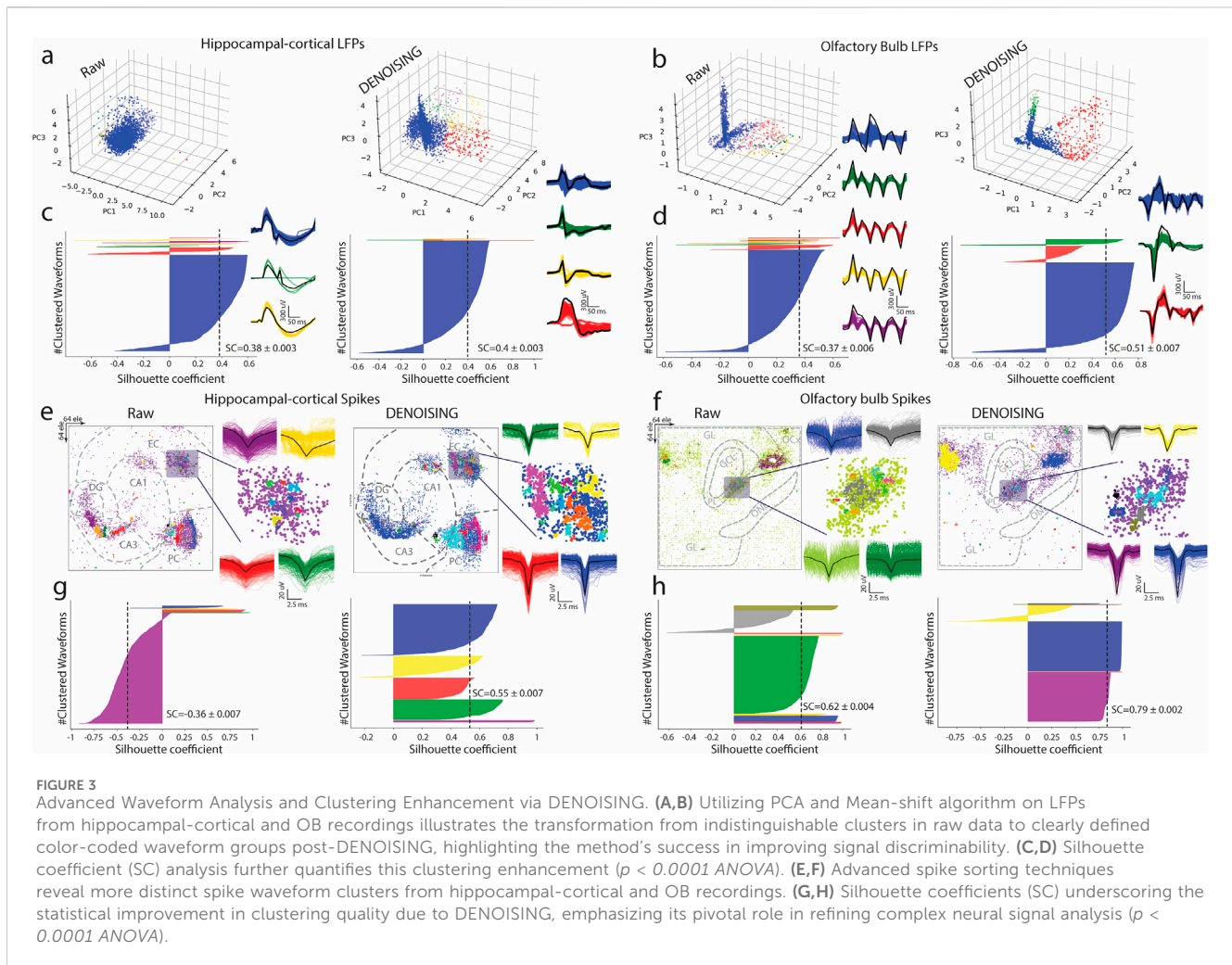
To further evaluate the impact of our DENOISING method, we applied PCA and the Mean-Shift algorithm to LFPs extracted from raw and denoised hippocampal and OB recordings. On raw data, PCA depicted a jumbled cluster of signals, indicating a lack of distinct grouping among waveform features. However, post-DENOISING, PCA delineated between groups of data, with color-coded waveforms distinctly belonging to their respective clusters (Figures 3A, B). This stark differentiation underscores DENOISING's capability to significantly enhance the discriminability and clarity of neural signals, allowing for a more nuanced interpretation of complex network activities.

Furthermore, silhouette coefficient analysis quantitatively confirmed the superior clustering performance in denoised data over raw recordings (Figures 3C, D).

Expanding our analysis, we employed an advanced spike sorting technique to scrutinize spiking activities within these recordings (Hilgen et al., 2017). This process also benefited markedly from the DENOISING process, revealing more defined and distinguishable clusters of spike waveforms. These were coherently matched with their groups identified through PCA maps, reinforcing the denoising method's effectiveness (Figures 3E, F). The application of silhouette coefficients re-emphasized a statistical foundation for asserting the significant enhancement in clustering quality attributable to our denoising technique, underscoring its effectiveness in refining the analysis of complex neural signals (Figures 3G, H).

3.4 Benchmarking with traditional noise removal approaches

Employing SNR distribution analysis, calculated as the mean over standard deviation, we observed a pronounced enhancement in both LFP and spiking activity data post-DENOISING (Figures 4A–D). Specifically, the SNR in hippocampal-cortical and OB LFPs denoised data yielded a 38.8 and 53-fold increase,



respectively, over raw data (Figures 4A, B). Similarly, spiking activity analysis revealed significant gains, with a 78.8-fold increase in hippocampal-cortical regions and a 16-fold improvement in OB regions (Figures 4C, D).

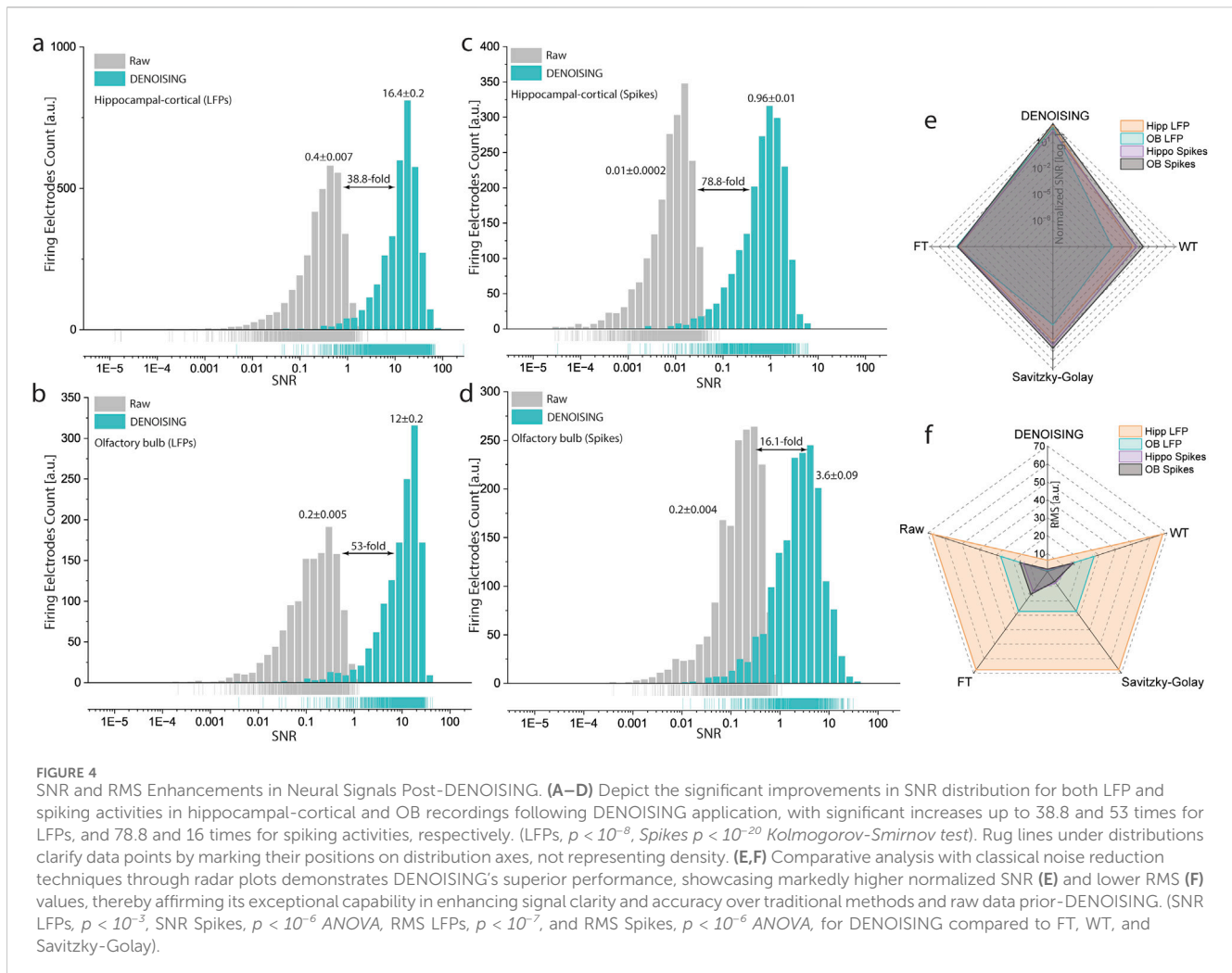
While classical noise reduction methods have not been explicitly documented in the context of large-scale extracellular recordings and HD-MEAs, we aimed to rigorously evaluate the performance of DENOISING compared to these established techniques—specifically, Wavelet Transform, Fourier Transform, and Savitzky-Golay filter. Our objective was to comprehensively assess DENOISING's efficacy in enhancing signal clarity and accuracy, which is critical for deciphering the nuanced dynamics of neural activity within the hippocampal-cortical and OB networks.

Further comparative analysis employed the RMS parameter and normalized SNR of denoised data to raw, illustrating DENOISING's superiority. Radar plots displayed that denoised data exhibited significantly higher SNR (Figure 4E) and lower RMS values (Figure 4F) for both LFPs and spikes, outperforming classical noise-removal methods. These findings underscore the advanced capability of DENOISING in refining neural signal analysis, setting a new benchmark for the analysis of complex extracellular recordings.

4 Discussion

We have introduced DENOISING, a computational framework validated with experimental multimodal data to enhance fidelity and clarity through dynamic noise mitigation on large-scale bioelectrical signals. The adaptive nature of the method allowed for handling a wide range of noise, including electrical, mechanical, and environmental sources, ensuring robust noise removal while preserving the essential features of a diverse array of extracellular LFP and spike signals. This capability is particularly relevant in the context of recent advancements in large-scale biosensing HD-MEAs and their application in monitoring neural dynamics across various spatial and temporal scales. By facilitating precise observations of network-wide activity, our approach enabled a deeper understanding of the interconnected processes governing brain function, which has profound implications for areas critical to learning, memory, and sensory processing.

Central to our results is the improved accuracy in waveform clustering, spike sorting, and CAT analysis, allowing for more precise identification and categorization of neural signals and network dynamics. This precision is critical for understanding the nuanced activities within neural circuits and contributes to a more explicit interpretation of neural communication patterns.



Through significant SNR improvements and RMS noise reduction analyses, our methodology provided compelling evidence of its performance that transcends traditional methods. This enhancement not only improved the quality and reliability of neural data but also enabled the detection of subtle neural activity, thus unveiling obscured neural dynamics and interactions that were previously indiscernible.

Furthermore, our study aligns with the growing body of research emphasizing the critical need for high-fidelity neural data to understand complex brain functions and disorders (Hu et al., 2022; Emery et al., 2023a; Li et al., 2023; Vázquez-Guardado et al., 2020), necessitating multi-purpose denoising methods (Lecoq et al., 2021; Eom et al., 2023; Li et al., 2021).

In addressing the specific process of our DENOISING method, it is important to clarify that while the algorithm proficiently identifies and improves the clarity of signals associated with significant LFP and spike events, it does not alter or reconstruct signal components outside of these detected events. This is evident in Figure 2, where only meaningful neural activities are highlighted, emphasizing the adaptive nature of our filter in focusing on significant neural events. This selective filtering is vital for accurately interpreting SNR improvements

shown in Figure 4, as it directly relates to the assessed signal quality rather than indiscriminately altering the entire data spectrum.

While the DENOISING framework has shown substantial efficacy in enhancing the clarity of extracellular recordings through dynamic adjustment and noise separation, it does not incorporate the application of deep learning approaches exemplified by other methods (Lecoq et al., 2021; Eom et al., 2023; Li et al., 2021). However, by not utilizing a machine learning backbone or extensive training datasets, DENOISING offers a significant computational advantage compared to other methods. It requires considerably less computational resources and time, bypassing the need to train a neural network, which is computationally intensive and requires large datasets. This makes DENOISING more accessible for real-time applications and suitable for environments with limited computational capabilities, providing a practical solution for immediate noise reduction without the overhead of training and model optimization. However, integrating a deep learning component into our framework represents a compelling avenue for future research, which could potentially offer improved adaptability and precision in noise reduction and signal

processing by harnessing the power of large-scale neural datasets for training purposes.

Data availability statement

The datasets presented in this study can be found in online repositories. The names of the repository/repositories and accession number(s) can be found in the article/supplementary material.

Ethics statement

The animal study was reviewed and approved by the committee of the official state Directorate Saxony authority responsible for animal testing (approval number 25–5131/476/14).

Author contributions

XH: Data curation, Formal Analysis, Investigation, Software, Writing–review and editing, Methodology. BA: Formal Analysis, Investigation, Methodology, Writing–review and editing. SK: Investigation, Methodology, Writing–review and editing. HA: Conceptualization, Data curation, Formal Analysis, Funding acquisition, Investigation, Methodology, Project administration, Resources, Software, Supervision, Validation, Visualization, Writing–original draft, Writing–review and editing.

References

- Amin, H., Maccione, A., Marinaro, F., Zordan, S., Nieuw, T., and Berdondini, L. (2016). Electrical responses and spontaneous activity of human iPSC-derived neuronal networks characterized for 3-month culture with 4096-electrode arrays. *Front. Neurosci.* 10 (121), 1–15. doi:10.3389/fnins.2016.00121
- Amin, H., Marinaro, F., Tonelli, D. P., and Berdondini, L. (2017b). Developmental excitatory-to-inhibitory GABA-polarity switch is disrupted in 22q11.2 deletion syndrome: a potential target for clinical therapeutics. *Sci. Rep.* 7 (1), 1–18. doi:10.1038/s41598-017-15793-9
- Amin, H., Nieuw, T., Lonardoni, D., Maccione, A., and Berdondini, L. (2017a). High-resolution bioelectrical imaging of A β -induced network dysfunction on CMOS-MEAs for neurotoxicity and rescue studies. *Sci. Rep.* 7 (1), 2460. doi:10.1038/s41598-017-02635-x
- Bathellier, B., Buhl, D. L., Accolla, R., and Carleton, A. (2008). Dynamic ensemble odor coding in the mammalian olfactory bulb: sensory information at different timescales. *Neuron* 57 (4), 586–598. doi:10.1016/j.neuron.2008.02.011
- Berdondini, L., Imfeld, K., Maccione, A., Tedesco, M., Neukom, S., Koudelka-Hep, M., et al. (2009). Active pixel sensor array for high spatio-temporal resolution electrophysiological recordings from single cell to large scale neuronal networks. *Lab. Chip* 9 (18), 2644–2651. doi:10.1039/b907394a
- Bird, C. M., and Burgess, N. (2008). The hippocampus and memory: insights from spatial processing. *Nat. Rev. Neurosci.* 9 (3), 182–194. doi:10.1038/nrn2335
- Buzsáki, G. (1989). Two-stage model of memory trace formation: a role for “noisy” brain states. *Neuroscience* 31 (3), 551–570. doi:10.1016/0306-4522(89)90423-5
- Buzsáki, G. (2004). Large-scale recording of neuronal ensembles. *Nat. Neurosci.* 7 (5), 446–451. doi:10.1038/nn1233
- Buzsáki, G., Anastassiou, C. A., and Koch, C. (2012). The origin of extracellular fields and currents-EEG, ECoG, LFP and spikes. *Nat. Rev. Neurosci.* 13 (6), 407–420. doi:10.1038/nrn3241
- Coates, A., and Ng, A. Y. (2012). Learning feature representations with K-means. *Lect. Notes Comput. Sci. Incl. Subser. Lect. Notes Artif. Intell. Lect. Notes Bioinforma.* 7700, 561–580. doi:10.1007/978-3-642-35289-8_30
- Cole, S. R., and Voytek, B. (2017). Brain oscillations and the importance of waveform shape. *Trends Cogn. Sci.* 21 (2), 137–149. doi:10.1016/j.tics.2016.12.008
- Comaniciu, D., and Meer, P. (2002). Mean shift: a robust approach toward feature space analysis. *IEEE Trans. Pattern Anal. Mach. Intell.* 24 (5), 603–619. doi:10.1109/34.1000236
- Czanner, G., Sarma, S. V., Ba, D., Eden, U. T., Wu, W., Eskandar, E., et al. (2015). Measuring the signal-to-noise ratio of a neuron. *Proc. Natl. Acad. Sci. U. S. A.* 112 (23), 7141–7146. doi:10.1073/pnas.1505545112
- Donoho, D. L. (1995). De-noising by soft-thresholding. *IEEE Trans. Inf. Theory* 41 (3), 613–627. doi:10.1109/18.382009
- Emery, B. A., Hu, X., Khanzada, S., Kempermann, G., and Amin, H. (2023a). High-resolution CMOS-based biosensor for assessing hippocampal circuit dynamics in experience-dependent plasticity. *Biosens. Bioelectron.* 237 (5), 115471. doi:10.1016/j.bios.2023.115471
- Emery, B. A., Hu, X., Maugeri, L., Khanzada, S., Klütsch, D., and Amin, H. (2022). Large-scale multimodal neural recordings on a high-density neurochip: olfactory bulb and hippocampal networks. *IEEE EMBS*, 42–45. doi:10.1109/EMBC48229.2022.9871961
- Emery, B. A., Khanzada, S., Hu, X., Rossi, L., Klütsch, D., Altuntac, E., et al. (2023b). “Recording network-based synaptic transmission and LTP in the hippocampal network on a large-scale biosensor,” in *2023 IEEE BioSensors conference (BioSensors)* (IEEE), 1–4. Available at: <https://ieeexplore.ieee.org/document/10280958/>.
- Eom, M., Han, S., Park, P., Kim, G., Cho, E. S., Sim, J., et al. (2023). Statistically unbiased prediction enables accurate denoising of voltage imaging data. *Nat. Methods* 20 (10), 1581–1592. doi:10.1038/s41592-023-02005-8
- Gustafsson, F. (1996). Determining the initial states in forward-backward filtering. *IEEE Trans. Signal Process.* 44 (4), 988–992. doi:10.1109/78.492552
- Harris, K. D., Henze, D. A., Csicsvari, J., Hirase, H., and Buzsáki, G. (2000). Accuracy of tetrode spike separation as determined by simultaneous intracellular and extracellular measurements. *J. Neurophysiol.* 84 (1), 401–414. doi:10.1152/jn.2000.84.1.401

Funding

The author(s) declare that financial support was received for the research, authorship, and/or publication of this article. This study was financed from basic institutional funds (DZNE) and partly from the Helmholtz Validation Fund (HVF-012).

Acknowledgments

We want to acknowledge the support of the platform for behavioral animal testing at the DZNE-Dresden (Dr. Alexander Garthe, Anne Karasinsky, Sandra Günther, and Jens Bergmann).

Conflict of interest

The authors declare that the research was conducted in the absence of any commercial or financial relationships that could be construed as a potential conflict of interest.

Publisher’s note

All claims expressed in this article are solely those of the authors and do not necessarily represent those of their affiliated organizations, or those of the publisher, the editors and the reviewers. Any product that may be evaluated in this article, or claim that may be made by its manufacturer, is not guaranteed or endorsed by the publisher.

- Hilgen, G., Sorbaro, M., Pirmoradian, S., Muthmann, J. O., Kepiro, I. E., Ullo, S., et al. (2017). Unsupervised spike sorting for large-scale, high-density multielectrode arrays. *Cell Rep.* 18 (10), 2521–2532. doi:10.1016/j.celrep.2017.02.038
- Hu, X., Khanzada, S., Klütsch, D., Calegari, F., and Amin, H. (2022). Implementation of biohybrid olfactory bulb on a high-density CMOS-chip to reveal large-scale spatiotemporal circuit information. *Biosens. Bioelectron.* 198 (3), 113834. doi:10.1016/j.bios.2021.113834
- Hyndman, R. J., and Koehler, A. B. (2006). Another look at measures of forecast accuracy. *Int. J. Forecast.* 22 (4), 679–688. doi:10.1016/j.ijforecast.2006.03.001
- Kay, K. (2022). The risk of bias in denoising methods: examples from neuroimaging. *PLoS One* 17 (7), 1–19. doi:10.1371/journal.pone.0270895
- Kempermann, G., Gage, F. H., Aigner, L., Song, H., Curtis, M. A., Thuret, S., et al. (2018). Human adult neurogenesis: evidence and remaining questions. *Cell Stem Cell* 23 (1), 25–30. doi:10.1016/j.stem.2018.04.004
- Krishnan, S. R., and Seelamantula, C. S. (2013). On the selection of optimum Savitzky-Golay filters. *IEEE Trans. Signal Process.* 61 (2), 380–391. doi:10.1109/tsp.2012.2225055
- Lecoq, J., Oliver, M., Siegle, J. H., Orlova, N., Ledochowitsch, P., and Koch, C. (2021). Removing independent noise in systems neuroscience data using DeepInterpolation. *Nat. Methods* 18 (11), 1401–1408. doi:10.1038/s41592-021-01285-2
- Lepousez, G., Valley, M. T., and Lledo, P. M. (2013). The impact of adult neurogenesis on olfactory bulb circuits and computations. *Annu. Rev. Physiol.* 75 (1), 339–363. doi:10.1146/annurev-physiol-030212-183731
- Li, H., Wang, J., and Fang, Y. (2023). Recent developments in multifunctional neural probes for simultaneous neural recording and modulation. *Microsyst. Nanoeng.* 9 (1), 4. doi:10.1038/s41378-022-00444-5
- Li, X., Zhang, G., Wu, J., Zhang, Y., Zhao, Z., Lin, X., et al. (2021). Reinforcing neuron extraction and spike inference in calcium imaging using deep self-supervised denoising. *Nat. Methods* 18 (11), 1395–1400. doi:10.1038/s41592-021-01225-0
- Lisman, J. (2005). The theta/gamma discrete phase code occurring during the hippocampal phase precession may be a more general brain coding scheme. *Hippocampus* 15 (7), 913–922. doi:10.1002/hipo.20121
- Lisman, J., Buzsáki, G., Eichenbaum, H., Nadel, L., Ranganath, C., and Redish, A. D. (2017). Viewpoints: how the hippocampus contributes to memory, navigation and cognition. *Nat. Neurosci.* 20 (11), 1434–1447. doi:10.1038/nn.4661
- Luo, M., and Katz, L. C. (2001). Response correlation maps of neurons in the mammalian olfactory bulb. *Neuron* 32 (6), 1165–1179. doi:10.1016/s0896-6273(01)00537-2
- Minka, T. P. (2008). *Automatic dimensionality selection for PCA*.
- Mori, K., Nagao, H., and Yoshihara, Y. (1999). The olfactory bulb: coding and processing of odor molecule information. *Sci. (1979)* 286 (5440), 711–715. doi:10.1126/science.286.5440.711
- Müller, J., Ballini, M., Livi, P., Chen, Y., Radivojevic, M., Shadmani, A., et al. (2015). High-resolution CMOS MEA platform to study neurons at subcellular, cellular, and network levels. *Lab. Chip* 15 (13), 2767–2780. doi:10.1039/c5lc00133a
- Patil, R. (2015). Noise reduction using wavelet transform and singular vector decomposition. *Procedia Comput. Sci.* 54, 849–853. doi:10.1016/j.procs.2015.06.099
- Rossi, L., Emery, B. A., Khanzada, S., Hu, X., and Amin, H. (2023). “Pharmacologically and electrically-induced network-wide activation of olfactory bulb with large-scale biosensor,” in *2023 IEEE BioSensors conference (BioSensors) (IEEE)*, 1–4. Available at: <https://ieeexplore.ieee.org/document/10280876/>.
- Rousseeuw, P. J. (1987). Silhouettes: a graphical aid to the interpretation and validation of cluster analysis. *J. Comput. Appl. Math.* 20 (C), 53–65. doi:10.1016/0377-0427(87)90125-7
- Scharfman, H. E. (2007). The CA3 “backprojection” to the dentate gyrus. *Prog. Brain Res.* 163 (07), 627–637. doi:10.1016/S0079-6123(07)63034-9
- Starck, J. L., Candès, E. J., and Donoho, D. L. (2002). The curvelet transform for image denoising. *IEEE Trans. Image Process.* 11 (6), 670–684. doi:10.1109/tip.2002.1014998
- Vázquez-Guardado, A., Yang, Y., Bhandokar, A. J., and Rogers, J. A. (2020). Recent advances in neurotechnologies with broad potential for neuroscience research. *Nat. Neurosci.* 23 (12), 1522–1536. doi:10.1038/s41593-020-00739-8
- Vyas, S., Golub, M. D., Sussillo, D., and Shenoy, K. V. (2020). Computation through neural population dynamics. *Annu. Rev. Neurosci.* 43, 249–275. doi:10.1146/annurev-neuro-092619-094115